ELSEVIER

International Journal of Heat and Fluid Flow 22 (2001) 237–244

International Journal of
HEAT AND
FLUID FLOW

www.elsevier.com/locate/ijhff

Direct numerical simulation of rough-wall heat transfer in a turbulent channel flow

Yutaka Miyake *, Koichi Tsujimoto, Masaru Nakaji

Department of Mechanical Engineering, Osaka University, 2-1, Yamada-oka, Suita, Osaka 565-0871, Japan

Abstract

Heat transfer in a channel of rough wall is simulated in this work. Two kinds of roughness are considered, i.e., one assumes sand-grain roughness based on roughness model and the other regularly arranged two-dimensional ribs. No models other than sand-grain roughness implemented in the simulation. For the sake of computational load, one wall is assumed to be smooth and the global Reynolds number Re_τ based on mean friction velocity and half channel width is 150. Mean flow property of velocity and thermal fields are found to be little influenced by the property of roughness elements but depends on total drag, except for in the layer close to the wall where direct interference with roughness elements manifests itself. Similarity of thermal field with velocity one is confirmed for the low Prandtl number flows considered in the work. The mixing is found to be controlled by large scale motion which is inherent to the logarithmic layer, getting closer to the wall.

Keywords: Channel flow; Turbulence; Rough wall; DNS; Convective heat transfer

1. Introduction

Heat transfer on a rough wall is of keen interest in engineering practice as most of heat exchanging solid surfaces are more or less rough. So, fundamental mechanism of the role of roughness on heat transfer is hoped to be understood more in detail. Direct numerical simulation (DNS) is capable of reproducing thermo-fluid field with extremely high resolution and gives detailed structures of related phenomena which are never obtained by experiments. However, it is only in recent days that rough-wall turbulent flow was calculated by DNS, even for just flow field without heat transfer. This is because the additional computational load caused by subjecting the non-slip condition at every point on the indented surface becomes prohibitively large compared with the ability of available computers. To simulate a turbulent flow implementing thermal field over a rough wall is still far beyond the scope of DNS, if practical turbulent flows of the high Reynolds number are treated.

First DNS of rough-wall turbulent flow was published by the present authors (Miyake et al., 1999), though a model had to be used in order to represent roughness element. The DNS dealt with sand-grain roughness and gave reasonable reproduction of rough-wall property, e.g., the downward shift of straight line of logarithmic mean velocity distribution whose magnitude is within experimental scatter and thinning of viscous sublayer disappears. It has been confirmed that the wall drag on a rough wall is composed of much larger profile drag than friction drag and that turbulent property inherent to logarithmic layer comes closer to the wall. Since friction drag generates stronger velocity fluctuation than the same magnitude of profile drag does, turbulence looks suppressed on a rough-wall flow compared with on a smooth-wall flow when normalized by total drag, contrary to the intuition. The correct interpretation of the result, however, gives enhancement of turbulence by roughness.

These encouraging results motivated us to conduct more detailed simulation of the near-wall turbulence over the rough wall than previous one and to implement heat transfer to investigate the mechanism of its enhancement. In this work, two DNSs are conducted. One is the extension of previous DNS of a sand-grain roughness wall flow accompanying heat transfer and the other is a turbulent channel flow having k-type roughness of periodically arranged two-dimensional spanwise ribs of square cross-section with heat transfer. The latter case is treated without any model and is a pure DNS. This simulation is mainly to understand the physics of a heat transfer process, though limited in a very low Reynolds number case. On the other hand it is intended as well to present a standard database to help inventing more simplified but trustful models for roughness effect, in order to meet the demands from engineering application. DNS for a sand-grain roughness case is an example to exemplify a simplified model and is included in this work to zoom up its prospect and drawback as well. Physics inherent to the rough wall is also discussed.

* Corresponding author. Tel.: +81-6-6879-7248; fax: +81-6-6876-7250.

E-mail address: miyake@mech.eng.osaka-u.ac.jp (Y. Miyake).

0142-727X/01/$ - see front matter
PII: S0142-727X(01)00085-6

Notation

a	thermal diffusivity
a_t	turbulent thermal diffusivity, $-\overline{v'T'}/(\mathrm{d}\bar{T}/\mathrm{d}y)$
c_p	specific heat at constant pressure
H	half channel width
H_r	distance of the plane of vanishing turbulent shear stress from the rough wall
h_s	height of roughness
k	turbulent kinetic energy, $\overline{u'_k u'_k}/2$
Nu	Nusselt number
Pr	Prandtl number, ν/a
Pr_t	turbulent Prandtl number, ν_t/a_t
p	pressure
q_w	wall heat flux, $\lambda(\mathrm{d}T/\mathrm{d}y)\|_{wall}$
Re_τ	global Reynolds number, $\bar{u}_\tau H/\nu$
$Re_{\tau,r}$	equivalent global Reynolds number of the flow over a rough wall, $\bar{u}_{\tau,r}H_r/\nu$
r	ratio of turbulent shear stress to turbulent kinetic energy, $-\overline{u'v'}/k$
S_v	skewness factor of wall normal velocity, $\overline{v'^3}/v'^3_{rms}$
T	temperature
T_b	global mean temperature, $\int_0^{H_r} u(T-T_w)\,\mathrm{d}y/\int_0^{H_r} u\,\mathrm{d}y + T_w$
T_w	temperature of rough wall
T_l	temperature of smooth wall
t	time
$\bar{t}_\tau$	mean friction temperature, $q_w/\rho c_p \bar{u}_\tau$
$\bar{t}_{\tau,r}$	mean friction temperature, $q_w/\rho c_p \bar{u}_{\tau,r}$ on the rough wall
u, v, w	velocity components in x, y, and z directions, respectively
$\bar{u}_\tau$	global mean friction velocity, $\bar{u}_\tau = [(H/\rho)(\mathrm{d}\bar{p}/\mathrm{d}x)]^{1/2}$
$\bar{u}_{\tau,r}$	global mean friction velocity defined on the rough wall
x, y, z	axis in streamwise, wall-normal and spanwise directions, respectively
y^+	non-dimensional distance from wall, $\bar{u}_\tau y/\nu$
y_r^+	non-dimensional distance from wall, $\bar{u}_{\tau,r}y/\nu$ on the rough wall
y_r^*	global coordinate, y/H_r
α	heat transfer coefficient
λ	thermal conductivity
ν	kinematic viscosity
ν_t	turbulent kinematic viscosity, $-\overline{u'v'}/(\mathrm{d}\bar{u}/\mathrm{d}y)$
ρ	density
θ	non-dimensionalized temperature, $(T-T_w)/(T_l-T_w)$
θ_b	non-dimensionalized global mean temperature, $(T_b-T_w)/(T_l-T_w)$
$\bar{\theta}_{\tau,r}$	normalized global mean temperature, $\bar{\theta}_{\tau,r} = \bar{t}_{\tau,r}/(T_l-T_w)$ on the rough wall
$(A)^+$	non-dimensionalized quantity $(\overline{A})$ by $\bar{u}_{\tau,r}$, ν and $\bar{\theta}_{\tau,r}$
$(\overline{A})$	ensemble average over x, z-direction and time
$(A)'$	fluctuating component
$(A)_{rms}$	root-mean-square value

2. Computational procedure

2.1. Channels

Since implement of a roughness element in the calculation requires enormously high computational power, only one wall is assumed rough and the other wall is smooth. In the first case (Case 1), sand-grain roughness is assumed. Flow field of this rough wall is described in our previous paper (Miyake et al., 1999). The second case (Case 2) is for roughness of two-dimensional ribs of square cross-section, as illustrated in Fig. 1. A Cartesian coordinate system is employed, in which x, y, z are streamwise, normal, and spanwise directions, respectively, and the velocity components in the respective directions are denoted by u, v, w.

Computational conditions such as size of computational domain, grid number, Reynolds number and Prandtl number are given in Table 1(a) and (b) for Cases 1 and 2, respectively. The global Reynolds number is defined as $Re_\tau = \bar{u}_\tau H/\nu$, where

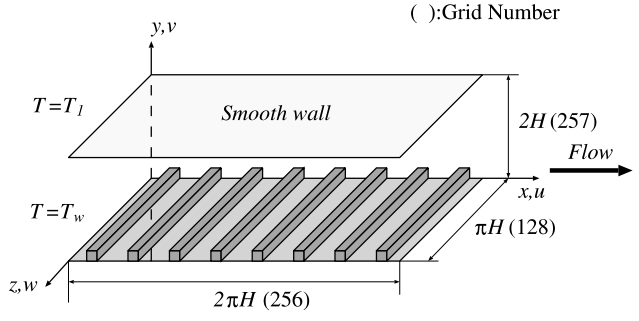

Fig. 1. Configuration of a channel with a rough wall of 2D ribs (Case 2).

$\bar{u}_\tau$ is global mean friction velocity and is calculated from pressure gradient $\mathrm{d}\bar{p}/\mathrm{d}x$ by $\bar{u}_\tau = [(H/\rho)(\mathrm{d}\bar{p}/\mathrm{d}x)]^{1/2}$, H is half channel width and ν and ρ are kinematic viscosity and density, respectively. As flow shifts to smooth-wall side because of smaller drag, equivalent Reynolds number based on mean friction velocity on each wall is different. Drag on the rough wall cannot be calculated directly and hence is estimated by subtracting that on the smooth wall from total drag of two walls.

As for the temperature field, both rough and smooth walls are iso-thermal walls and the temperature of rough wall is kept constant at T_w and that of smooth wall, at T_l. The temperature T is normalized to θ as $\theta = (T-T_w)/(T_l-T_w)$ in the calculation. Heat flux $\alpha(T_b - T_w)$ is equal to that at the wall calculated by $q_w = \lambda(\mathrm{d}T/\mathrm{d}y)|_{wall} = (T_b-T_w)(\lambda/\theta_b)(\mathrm{d}\theta/\mathrm{d}y)|_{wall}$, where α is the heat transfer coefficient. Global mean temperature T_b is calculated by $T_b - T_w = \int_0^{H_r} u(T-T_w)\,\mathrm{d}y/\int_0^{H_r} u\,\mathrm{d}y$, where H_r is the distance from the plane of vanishing turbulent shear stress to the rough wall, and this temperature difference $T_b - T_w$ is normalized to θ_b as $\theta_b = (T_b-T_w)/(T_l-T_w)$. Then, the Nusselt number Nu becomes

$$Nu = \frac{2H_r\alpha}{\lambda} = \frac{2Pr\cdot Re_{\tau,r}}{\theta_b^+}, \tag{1}$$

where $Pr = \nu/a$ is the Prandtl number and a is thermal diffusivity. $\theta_b^+ = (T_b-T_w)/\bar{t}_{\tau,r} = \theta_b/\bar{\theta}_{\tau,r}$ is the non-dimensionalized global mean temperature, where $\bar{t}_{\tau,r} = q_w/\rho c_p \bar{u}_{\tau,r}$ (c_p: specific heat at constant pressure) is friction temperature and $\bar{\theta}_{\tau,r} = \bar{t}_{\tau,r}/(T_l-T_w)$.

The spatial discretization is a Fourier series expansion in x and z for the sake of periodicity and a Chebyshev polynomial expansion in the normal direction. Time advancement is done by a semi-implicit method (Crank–Nicolson scheme for viscous term and third-order Adams–Bashforth scheme for the convective term).

Table 1
Computational conditions: (a) Case 1; (b) Case 2

	Streamwise	Wall normal	Spanwise
(a)			
Length	$4\pi H$	$2H$	πH
(wall unit)	(1885)	(300)	(471)
Grid number	128	129	64
Grid separation	14.7	0.045–3.68	7.36
Spectral mode	42	84	21
Reynolds number	$Re_r = H\bar{u}_r/\nu = 150$		
Prandtl number	$Pr = \nu/a = 0.71$		
(b)			
Length	$2\pi H$	$2H$	πH
(wall unit)	(942)	(300)	(471)
Grid number	256	257	128
Grid separation	3.68	0.011–1.84	3.68
Spectral mode	85	256	42
Reynolds number	$Re_r = H\bar{u}_r/\nu = 150$		
Prandtl number	$Pr = \nu/a = 0.71$		

2.2. Roughness element

The sand-grain roughness assumed in Case 1 of this DNS is represented by a line force $\boldsymbol{f}_v$ projected normal to the wall. The force is given by

$$\boldsymbol{f}_v = c_D \frac{1}{2}\rho \boldsymbol{v}|\boldsymbol{v}|\frac{A}{V}, \tag{2}$$

where A is the frontal area normal to local velocity $\boldsymbol{v}$, of the assumed roughness element and V is a volume of which a considering grid point represents. c_D is the drag coefficient for which $c_D = 2$ is adopted in this DNS. At each grid point along a line element of line force inside the roughness element, above force corresponding to the wall-normal height which the grid represents is added as an external concentrated point force in the momentum equation of fluid flow. The momentum equation normalized by $\bar{u}_\tau$ and H is

$$\frac{\partial \boldsymbol{v}}{\partial t} + (\boldsymbol{v}\cdot\nabla)\boldsymbol{v} = -\frac{1}{\rho}\nabla p + \frac{1}{Re_\tau}\nabla^2\boldsymbol{v} + \boldsymbol{f}_v. \tag{3}$$

It is assumed that the roughness elements are straight cones having basement radius of half spanwise grid separation and the height h_s^+ $(= h\bar{u}_\tau/\nu)$ has Gaussian distribution between $h_s^+ = 15$ and $h_s^+ = 40$ around its mean height $h_{sm}^+ = 25$. Except for this force, no additional condition to express non-slip behavior of fluid on the roughness element is applied but non-slip condition is subjected only on the solid wall planting roughness elements. It should be noted that the effects to the thermal field caused by these roughness elements such as increase of effective surface and that of heat exchange are not taken into account in the simulation of Case 1, except for resulting enhancement of mixing by roughness to the flow. The wall temperature is kept constant.

In Case 2 of this DNS, roughness is composed of periodically arranged two-dimensional spanwise ribs whose cross-section is square of a side $h_s^+ = 20$ and separated in streamwise direction by $\Delta x^+ = 118$. The boundary conditions on the solid wall are treated rigorously with respect to both non-slip flow and constant temperature. Namely, at each grid point $\boldsymbol{x}_s$ on every rib surface, external force $\boldsymbol{f}_v$ is added so as to make the flow vanishing. The magnitude of $\boldsymbol{f}_v$ is determined iteratively to satisfy

$$\boldsymbol{f}_v(\boldsymbol{x}_s, t) = \alpha_v \int_0^t \boldsymbol{v}(\boldsymbol{x}_s, t')\,\mathrm{d}t' + \beta_v \boldsymbol{v}(\boldsymbol{x}_s, t), \tag{4}$$

where α_v and β_v are negative constants to prevent the computation from instability and in this calculation, they are $\alpha_v = -4\times10^5$ and $\beta_v = -6\times10^2$. These procedures are proposed by Goldstein et al. (1995).

Similar treatment is required also for the computation of thermal field. Namely, in the equation for θ

$$\frac{\partial\theta}{\partial t} + (\boldsymbol{v}\cdot\nabla)\theta = \frac{1}{Pr\cdot Re_\tau}\nabla^2\theta + \boldsymbol{f}_\theta, \tag{5}$$

similar additional heat term $\boldsymbol{f}_\theta$ to keep the rib surface at prescribed temperature must be added. The way of determining $\boldsymbol{f}_\theta$ is the same as in Eq. (4), where $\alpha_\theta = -4\times10^5$ and $\beta_\theta = -6\times10^2$.

Additional operation to apply low pass filtering $K = \mathrm{e}^{\xi_2(n_x/N_x)^{\xi_1}}\mathrm{e}^{\xi_2(n_y/N_y)^{\xi_1}}\mathrm{e}^{\xi_2(n_z/N_z)^{\xi_1}}$ to the non-linear term $\boldsymbol{v}\times\boldsymbol{\omega}$ where $\boldsymbol{\omega} = \nabla\times\boldsymbol{v}$, $\boldsymbol{f}_v$ and $\boldsymbol{f}_\theta$ are needed to prevent computational instability, where n_i $(i = x, y, z)$ are modal number in each direction and N_i, total mode number. Magnitude of the constants ξ_1 and ξ_2 are 20 and -1, respectively, here.

3. Results

3.1. Mean flow and mean temperature

Mean velocity distributions are given in Fig. 2. In order to make the straight line of logarithmic part parallel to the one

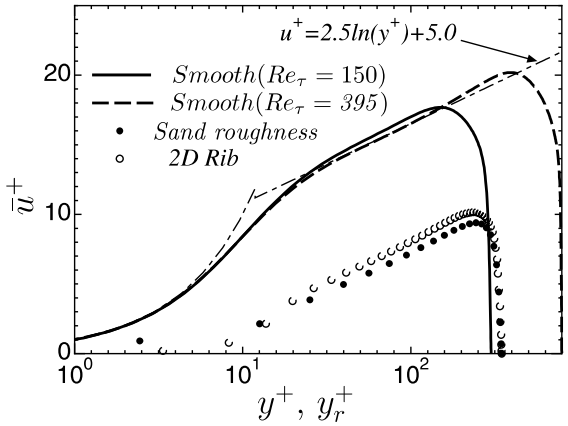

Fig. 2. Distribution of mean velocity $\bar{u}^+$ normalized by mean friction velocity $\bar{u}_{\tau,r}$ and ν.

established for the ordinary smooth flat wall, correction of the location of wall surface is required. In Case 1, however, this correction is not necessary but in Case 2, upward-shifting by $\Delta y^+ = 7.0$ is needed. Magnitude of the downward shift of the straight lines for both Cases 1 and 2 from the case of the ordinary smooth wall is within the scatter of experimental data (Raupach et al., 1991).

Corresponding shear stress distribution for Case 2 is given in Fig. 3. That in sand-grain roughness is reported in our previous report (Miyake et al., 1999). The equivalent half width of the rough-wall side H_r as defined above is larger than H because total drag on the rough wall is larger than on the smooth wall. In the following, equivalent Reynolds number $Re_{\tau,r}$ based on mean friction velocity on the rough wall $\bar{u}_{\tau,r}$ and thickness H_r will be occasionally used. It should be noted that $\bar{u}_{\tau,r}$ is not only for friction drag but also includes profile drag. $Re_{\tau,r}$ in both cases 1 and 2 are nearly equal and is about 260. The defect of total shear stress in the layer close to the rough wall found in Fig. 3 is covered by pressure drag of ribs. It is noted that local high viscous shear stress τ_{wr} is observed in the layer near the top of the rib surface. The fraction of profile drag D_r which is the integration of pressure difference between two vertical sides of a rib, of total drag D_w is 0.77. So, profile drag is dominant on the rough wall.

In order to demonstrate the numerical accuracy of the present DNS, the budget of turbulent kinetic energy and temperature variance in Case 2, are shown in Fig. 4. The residual term is negligibly small except for a few points near the rib height ($y^+ = 20$). It was confirmed that the residual term of equations of mean momentum and mean temperature, which are less sensitive to grid resolution than in turbulent kinetic energy and temperature variance, is also negligibly small.

Fig. 5 show (a) mean streamlines and (b) iso-contours of mean temperature in near-wall layer in one pitch of ribs of Case 2. The flow becomes nearly stagnant below $y^+ \simeq 20$ and on the vertical and top sides of a rib (surface 'A' in Fig. 3), high temperature gradient layer is formed. Since the mean stream is recirculating as shown in Fig. 3(a), the mean flow tends to upstream in the layer closest to the wall, and makes the wall friction negative, as observed at left-end side of Fig. 3.

Turbulent kinematic viscosity $\nu_t^+ = \nu_t/\nu = -\overline{u'v'}^+/(\mathrm{d}\bar{u}^+/\mathrm{d}y^+)$ varies to wall-normal direction as in Fig. 6, in which $\nu_t^+/Re_{\tau,r}$ versus y_r^* is shown. Lines are for smooth-wall flows of $Re_\tau = 150$ and 395 and symbols are for the rough-wall cases, • (Case 1), ◦ (Case 2). Good coincidence of the four curves demonstrates that $\bar{u}_{\tau,r}$ and y_r^* are representative velocity and length in the layer away from the wall for rough wall cases.

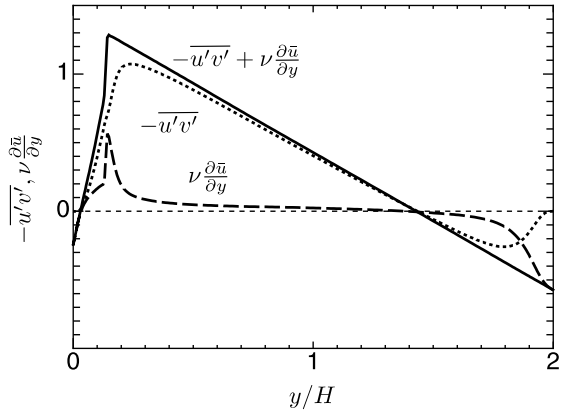

Fig. 3. Shear stress across channel with a rough wall of 2D ribs (Case 2), normalized by friction velocity $\bar{u}_\tau$ and ν.

The slight discrepancy of the lines for two smooth-wall flows demonstrates its Reynolds number dependency. Since two rough-wall cases are for nearly the same Reynolds number, they are totally coincident and close to high Reynolds number smooth-wall flow, except for in the layer close to the wall. This

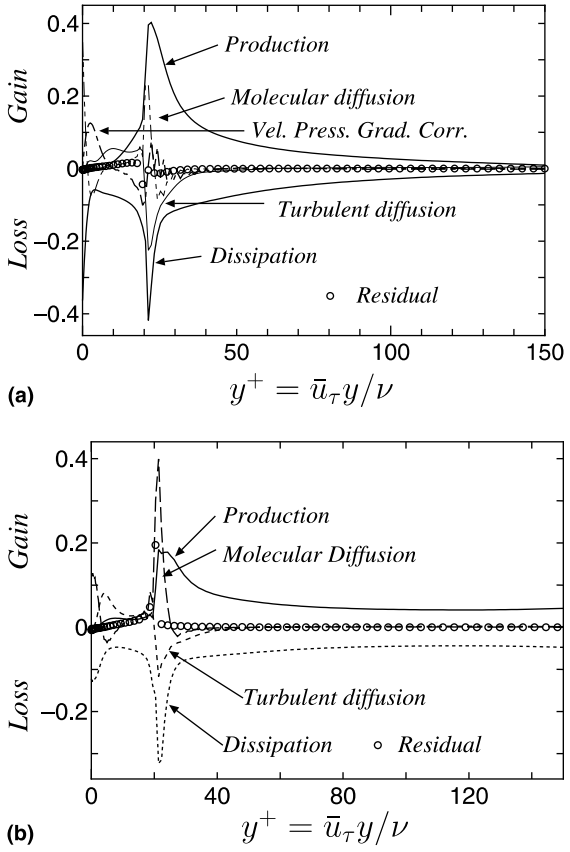

Fig. 4. Distribution of budget across the channel: (a) turbulent kinetic energy; (b) temperature variance. The axes are scaled by $\bar{u}_\tau$, $\bar{\theta}$ and ν.

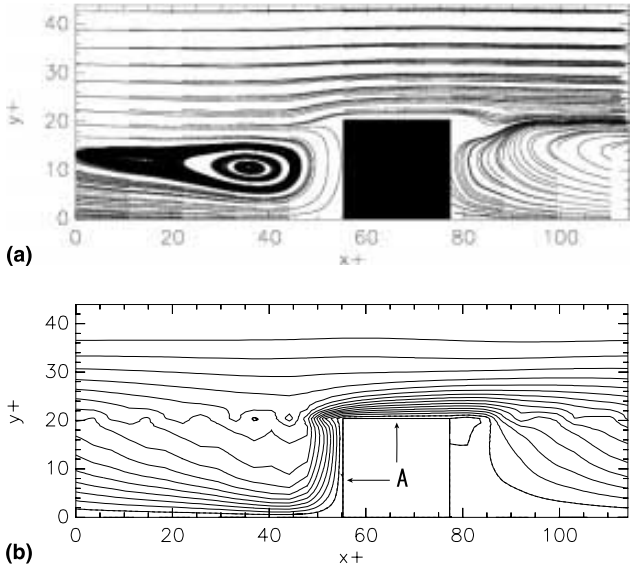

Fig. 5. Mean flow in one pitch of ribs near the rough wall of Case 2: (a) mean streamlines; (b) iso-contours of mean temperature.

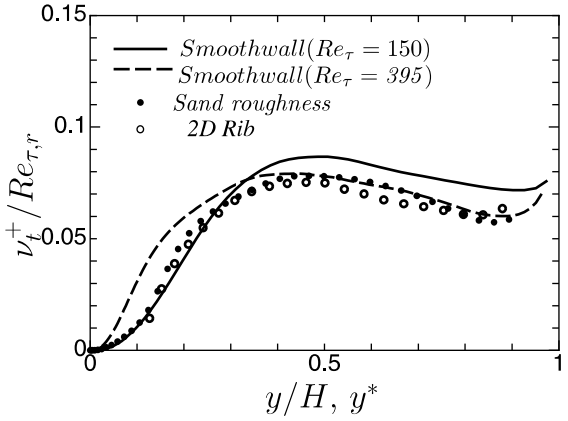

Fig. 6. Distribution of turbulent eddy viscosity $\nu_t/\bar{u}_{\tau,r}H_r$ over rough-wall flow of 2D ribs (Case 2).

confirms the fact that turbulence property in the layer farther a certain distance away from the wall is little influenced by the property of wall condition but the key is total drag, irrespective of friction drag or profile drag. It also suggests that the roughness equivalently raises the Reynolds number of the flow.

Mean temperature distribution $\bar{\theta}^+$ which is normalized by friction temperature $\bar{\theta}_{\tau,r}$ is shown in Fig. 7, where y^+ is taken in the horizontal axis in (a) and y/H_r (y/H, in smooth wall), in (b). Temperature field is dependent strongly on the Prandtl number, Reynolds number and thermal boundary conditions on the wall (Na et al., 1999; Kawamura et al., 1999) and similarity with velocity field is not expected as demonstrated by Kawamoto and Kawamura (1999).

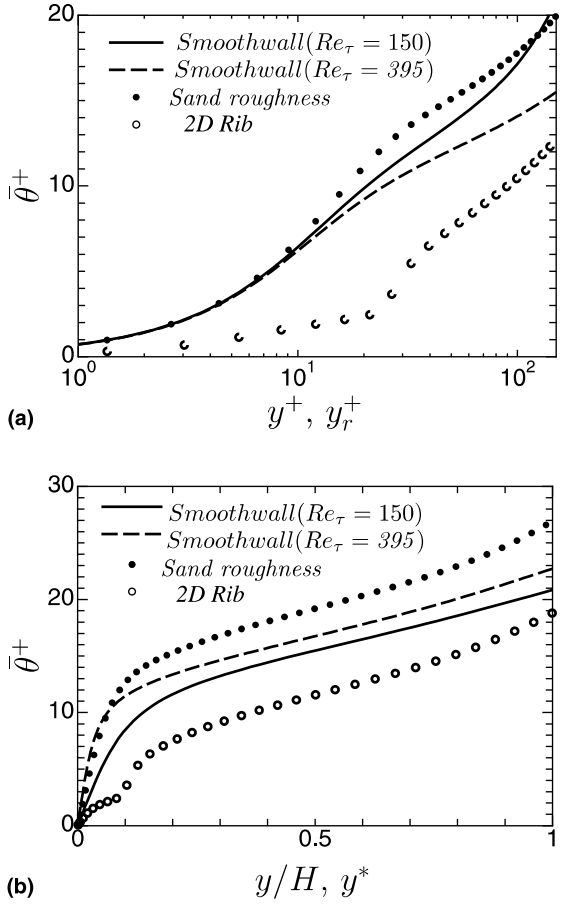

Fig. 7. Mean temperature distribution: (a) $\bar{\theta}^+$ vs. y^+; (b) $\bar{\theta}^+$ vs. $y/H_r, y/H$.

In Fig. 7(a), all curves of temperature distribution show similar distribution having straight line in the logarithmic layer, as the Prandtl number is as low as 0.7 in these DNSs. Viscous sublayer also appears except for the rib-roughness case (Case 2) and all three curves are identical. An interesting fact is that the friction temperature which is based not on friction drag but on total drag, works well as a scaling temperature in the sublayer. It is found that in the low Prandtl number flow over a smooth plate, the sublayers are nearly identical for flow and thermal fields. In the sand-grain roughness case, viscous sublayer is formed also in the thermal field as well as in the flow field. However, the sublayer in the former is identical with those over the smooth wall despite that the sublayer in the latter is not. This coincidence suggests that the heat flux is totally proportional to the friction temperature, in the layer near the wall, if no particular disturbance to represent additional stirring effect of roughness to the thermal field is implemented. In the layer above a couple of tens in wall unit from the wall, these three cases show different patterns. This is mainly because of the contamination of the thermal field by the wall of the other side, which is stronger in lower $Re_{\tau,r}$. The reason why the upward shift of the narrow layer of the logarithmic part is the largest for the sand-grain roughness case is again attributed to the fact that profile drag generates smaller turbulence than friction drag does, for the same magnitude of drag. The buffer layer looks slightly thickened in this scaling. The downward shift of the points in Case 2 can be attributed to the increase of heat exchange area by roughness elements whose effect is far larger than that due to smaller turbulence intensity of profile drag per unit drag than that of unit friction drag. In the two-dimensional rib, profile drag occupies larger fraction than friction drag, as mentioned earlier. The different tendency of the shift of Case 1 and Case 2 suggests strongly that implement of equivalent increase of heat-exchanging area is indispensable in estimating heat flux on a rough wall.

Fig. 7(b) demonstrates that influence of the wall condition manifests itself in the comparatively thin layer closest to the wall. So, in most of the channel width, a linear temperature profile which is nearly parallel regardless of the wall thermal conditions, appears. The vertical shift of the lines depends on the friction temperature $\bar{\theta}_{\tau,r}$. The asymmetric thermal field in the cases of the rough-wall channel affects slightly the temperature distribution in the central part of the channel.

Global enhancement of heat transfer by the rough wall is shown by the Nusselt number, those for two cases of rough and smooth-wall flows of $Re_\tau = 150, 395$ are shown in Fig. 8 in

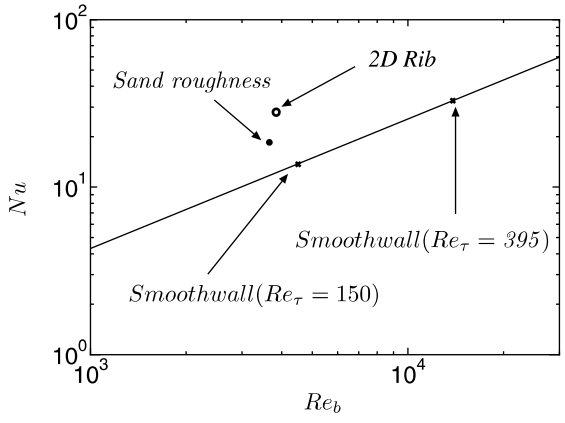

Fig. 8. Nusselt number for the present simulations.

which the horizontal axis is the Reynolds number based on mean global velocity $\bar{u}_b = \int_0^{H_r} u\,dy/H_r$. It is confirmed that the roughness enhances the heat transfer by comparing the points with established data for the smooth flat plate shown by a straight line (Kays and Crawford, 1980).

Distribution of heat flux non-dimensionalized by global mean friction velocity $\bar{u}_\tau$, global mean wall friction temperature $\bar{t}_\tau$ and ν across the channel is given in Fig. 9 for Case 2. Defect of total heat flux near the rough wall is covered by the horizontal heat transfer on the two vertical surfaces of ribs, as the profile drag does in the shear stress distribution.

Turbulent thermal diffusivity a_t is calculated by $a_t = -\overline{v'T'}/(d\bar{T}/dy)$. In Fig. 10, $a_t^+/Re_{\tau,r} = (a_t/\nu)/Re_{\tau,r} = -\overline{v'^+\theta'^+}/(d\bar{\theta}^+/dy^*)$ is shown taking y^* in the horizontal axis. These normalization are because that wall friction temperature $\bar{t}_{\tau,r}$ is adopted as the representative temperature and H_r, as that of length scale. It is confirmed also that non-dimensional thermal eddy diffusivity a_t^+ is again little affected by the property of roughness, as eddy viscosity ν_t shown in Fig. 6 is. The discrepancy between the smooth wall and the rough wall of the channel in the central part of the channel is due to contamination by the opposite side wall in the latter cases. High temperature thermal field in the smooth wall side in rough-wall channels makes the mean temperature distribution steeper than in symmetric smooth-wall cases, as shown in Fig. 7(b).

Distribution of the turbulent Prandtl number $Pr_t = \nu_t/a_t$ across the channel is nearly constant in most of the channel

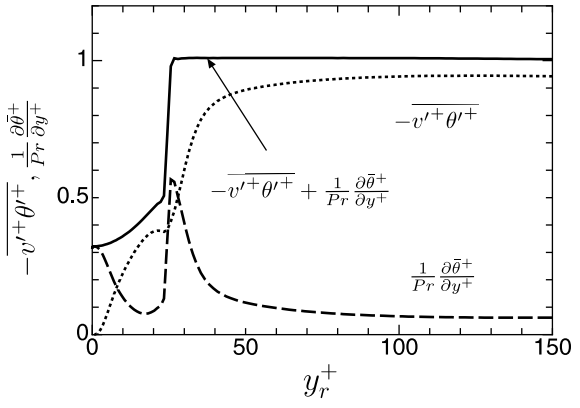

Fig. 9. Heat flux distribution over rough wall of 2D ribs, normalized by θ_τ and $\bar{u}_{\tau,r}$.

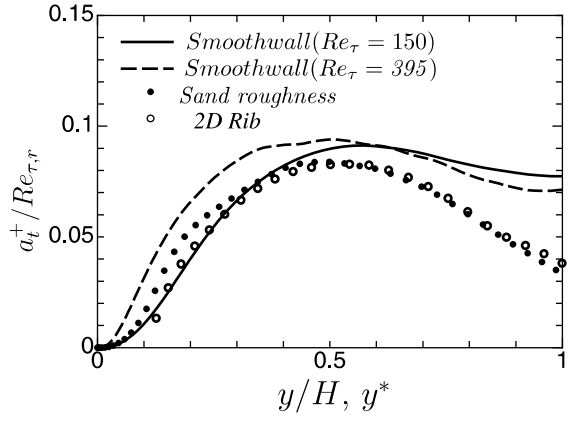

Fig. 10. Distribution of thermal diffusivity $a_t^+/Re_{\tau,r}$ over rough-wall flow of 2D ribs (Case 2).

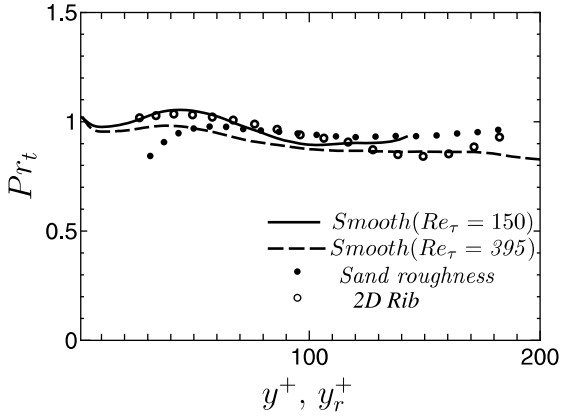

Fig. 11. Distribution of turbulent Prandtl number $Pr_t = \nu_t/a_t$ across the channel.

and is around unity, as shown in Fig. 11. Since in the central part of the channel, both shear stress and mean velocity gradient tend to zero and consequently estimation of ν_t is not reliable. So in Fig. 11, the central part of the channel is not included. The low Prandtl number makes the turbulence mixing for momentum and heat similar with each other.

3.2. Turbulent fluctuation

The ratio of turbulent shear stress $-\overline{u'v'}$ to turbulent kinetic energy k, $r = -\overline{u'v'}/k$ is known to be around 0.27 in the logarithmic layer and the larger the Reynolds number, the thicker the constant r-layer. The wall roughness makes this layer reach closer to the wall and this is confirmed also in Case 2 as shown in Fig. 12.

Temperature fluctuation $\theta'^+_{rms} = \theta'_{rms}/\bar{\theta}_{\tau,r}$ distributes to the wall-normal direction as shown in Fig. 13. Two smooth-wall cases reflect slight dependency of θ'^+_{rms} on the Reynolds number and the rough-wall cases are nearly coincident with each other except for in the layer close to the wall affected by roughness, which is consistent with Fig. 7(b) for mean temperature. Namely $\bar{t}_{\tau,r}$ is confirmed to be a good measure to represent turbulent mixing in the layer away from the wall. The steeper rise in the core region in rough-wall cases compared with smooth-wall channels is again the contamination by the field in the opposite side of the wall.

Similarity of momentum and heat transfer is demonstrated in Fig. 11. That is, the turbulent Prandtl number is around unity, which means that turbulent mixing of momentum and

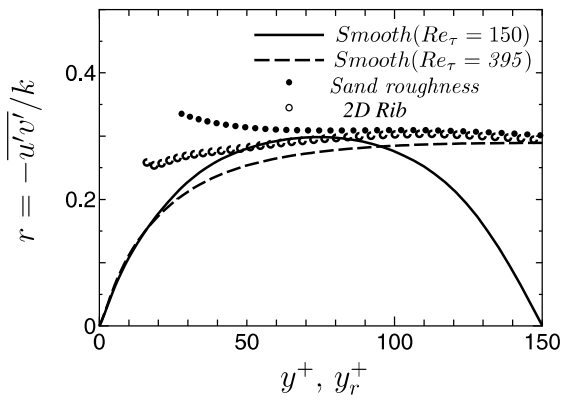

Fig. 12. Distribution of structure parameter $r = -\overline{u'v'}/k$.

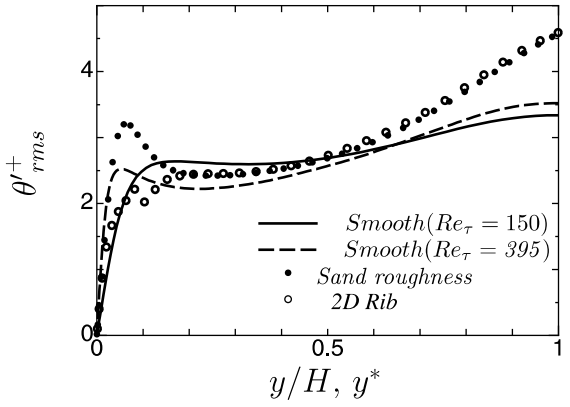

Fig. 13. Distribution of temperature fluctuation normalized by $\bar{\theta}_{\tau,r}$.

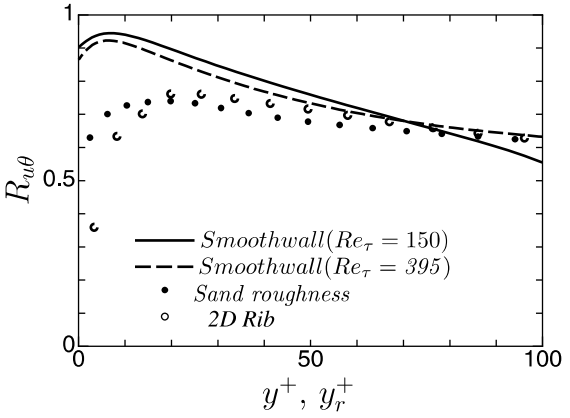

Fig. 14. Wall-normal distribution of temperature–streamwise velocity correlation coefficients, $R_{u\theta}$.

heat is quite similar. The correlation between fluctuations of streamwise velocity and temperature, $Re_{u\theta} = u'\theta'/u'_{\rm rms}\theta'_{\rm rms}$ which is shown in Fig. 14 confirms this similarity in a different way. Except for in the layer close to the wall, smooth-wall case of $Re_\tau = 395$ and two rough-wall cases are nearly coincident. The discrepancy near the wall suggests the difference of vortical systems in each flow. High correlation factor across the channel indicates that the vortices play a major role also in heat transfer. In an extremely low Reynolds number flow, however, it should be reminded that the core region manifests unmatured property in the sense of lack of the layer of constant-r for $Re_\tau = 150$ as shown in Fig. 12.

3.3. Structure of turbulence

As mentioned previously, the profile drag is dominant on the rough wall. However, in the region top of the roughness elements, the shear stress must be sustained mostly by turbulent shear flows. Therefore, strong turbulent mixing is required at the top of the ribs. While quasi-streamwise vortices generate this strong mixing near the smooth wall, different mechanism is expected to be dominant near the rough wall, since turbulence structure inherent to the layer away from the buffer layer comes closer to the wall in the latter, as suggested in Fig. 12. As the consequence, in place of streaks of mean spanwise separation $\Delta z^+ \sim 100$ which is distinguished feature of the buffer layer, large scale streaks of much larger mean spanwise separation than in the buffer layer appears, as shown in Fig. 15, where iso-surfaces of $|\Delta u^+| = 3.0$, negative in dark and positive in light gray are depicted. These large scale streaks are

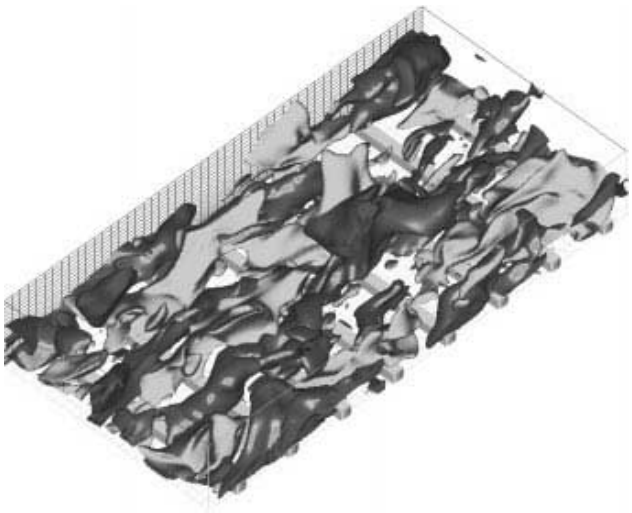

Fig. 15. 3D view of iso-surfaces of high and low streaks. Dark: $u'^+ = -3$; light gray: $u'^+ = 3$.

characteristic of wall turbulence of a large Reynolds number and accordingly, of the layer close to the wall near the rough surface. This modification of streaks suggests that quasi-streamwise vortices are not expected to play a dominant role in turbulent mixing in the near-wall layer.

In order to investigate the dominant mechanism of mixing, a conditional sampling technique is applied using skewness factor of wall normal velocity, $S_v = v'^3/v'^3_{\rm rms} = -15$ as the sampling signal. Fig. 16 compares iso-contours of fluctuation of wall-normal velocity over (a) smooth wall ($Re_\tau = 395$), (b)

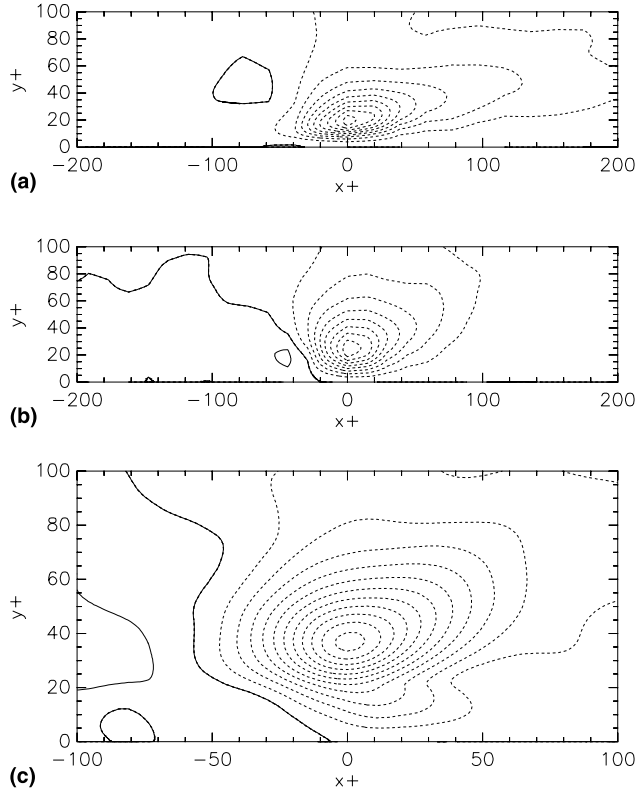

Fig. 16. Iso-contours of wall-normal velocity fluctuation corresponding to events of strong downwash: (a) smooth wall of $Re_\tau = 395$; (b) sand-grain roughness; (c) 2D rib ($|\Delta v'^+| = 0.2$).

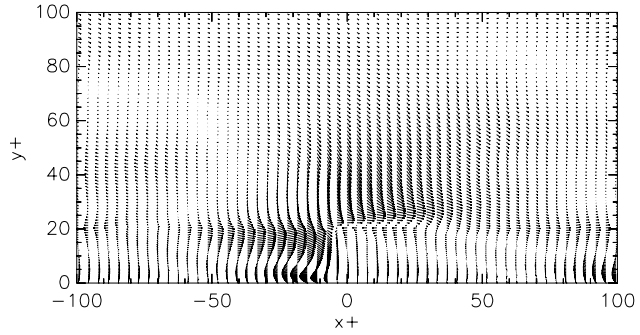

Fig. 17. Vector plots of conditional averaged velocity field corresponding to events of strong downwash in Case 2.

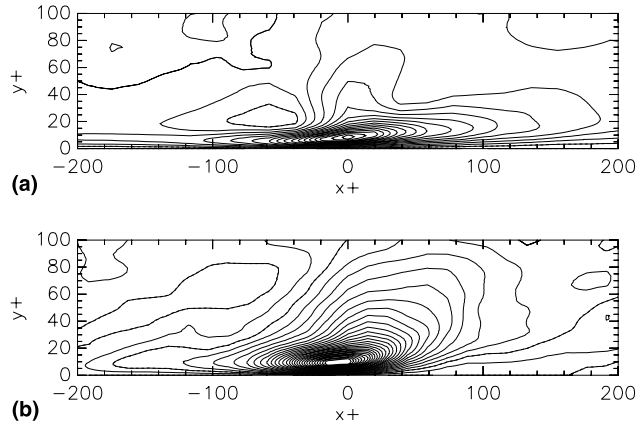

Fig. 18. Iso-contours of conditional averaged temperature fluctuation corresponding to events of strong downwash: (a) smooth wall of $Re_\tau = 395$; (b): sand-grain roughness, ($|\Delta\theta^+| = 0.2$).

rough wall of sand-grain roughness and (c) rough wall of two-dimensional ribs. The plane of detecting S_v is at $y^+ = y\bar{u}_\tau/\nu = 15$ in (a) and $y^+ = 35$ in (b) and (c). In the smooth-wall case, the curves are more flattened to vertical direction and more elongated in the streamwise direction than in the rough-wall cases. The vertical motion near the smooth wall detected in this manner represents mostly that caused by quasi-streamwise vortices. In the meantime, large scale motion spanning larger vertical distance is more important in rough-wall flows. That is, mixing between the layer close to the wall with the layer in the central part of the channel is more enhanced in the rough-wall flow compared with the smooth-wall flow. Buffer layer is to decouple the strong fluctuation with the laminar-like layer close to the wall. In case that turbulent fluctuation close to the wall is enhanced by the roughness element, strong fluctuation away from the wall can reach to close to the wall, though more or less suppressed. The mechanism of interaction between fluctuation close to the wall and the large-scale coherent motion away from the wall is not known at present. However, in the case of two-dimensional ribs, the strong downwash just upstream of a rib as the consequence of the recirculating flow shown in Fig. 5(a) enhance this mixing, as shown in Fig. 17 which is the same conditional averaged flow obtained by setting the detecting point at just upstream of the upstream-top corner of a rib.

Conditional averaged thermal field by the same sampling signal as in Fig. 16 gives Fig. 18 which shows the iso-contours of temperature fluctuation intensity θ^+ for (a) smooth wall ($Re_\tau = 395$) and (b) rough wall of sand-grain roughness (Case 1). The curves are quite similar to Figs. 16(a) and (b), suggesting that the heat transfer is mainly due to turbulent mixing as demonstrated in Figs. 11 and 14.

4. Conclusion

1. Turbulent channel flows with heat transfer of a low Prandtl number fluid are successfully reproduced for the rough wall of sand grains and two-dimensional ribs. In the layer away from the wall, both flow and the thermal fields are little affected by the condition of wall surface and enhanced eddy viscosity ν_t is scaled by equivalent channel width H_r and wall friction velocity $\bar{u}_{\tau,r}$ on the rough wall.

2. The thermal field has influence of opposite side field which is more when the Reynolds number is lower. In the layer close to the wall, logarithmic layer manifests itself for thermal field as well. Friction temperature $\bar{t}_\tau$ is a good scaling parameter for temperature distribution in the iso-thermal wall condition and for variance of temperature fluctuation, as well. However, implement of increase of heat exchanging solid surface by roughness elements is indispensable.

3. In the low Prandtl number fluid flow, the turbulent Prandtl number is nearly smooth and equal to unity and similarity of momentum and heat exchange is confirmed to hold for the rough wall as well.

4. The major effect of the roughness element is to modify the mechanism of turbulent mixing. Strong downwash spanning up to large distance from the wall plays a dominant role in enhancing mixing in the near-wall layer, in place of quasi-streamwise vortices in the buffer layer of the smooth-wall flow. Heat exchange is also controlled by this large-scale motion.

References

Goldstein, D., Handler, R., Sirovich, L., 1995. Direct numerical simulation of turbulent flow over a modeled riblet covered surface. J. Fluid Mech. 302, 598–606.

Kays, W.M., Crawford, M.E., 1980. Convective Heat and Mass Transfer, second ed. McGraw-Hill, New York.

Kawamura, H., Abe, H., Matsuo, Y., 1999. DNS of turbulent heat transfer in a channel flow with respect to Reynolds and Prandtl number effects. Int. J. Heat Fluid Flow 20, 196–207.

Kawamoto, N., Kawamura, H., 1999. DNS of turbulent heat transfer in a channel flow for different thermal boundary conditions. Trans. JSME 65 (637), 3117–3124 (in Japanese).

Miyake, Y., Tsujimoto, K., Agata, Y., 1999. A DNS of a turbulent flow in a rough-wall channel using roughness elements model. JSME Int. J. 43 (2), 233–242.

Na, Y., Papavassiliou, D.V., Hanratty, T.J., 1999. Use of direct numerical simulation to study the effect of Prandtl number on temperature effect. Int. J. Heat Fluid Flow 20, 187–195.

Raupach, M.R., Antonia, R.A., Rajagopalan, S., 1991. Rough-wall boundary layers. Appl. Mech. Rev. 44 (1), 1–25.